Numerical analysis of train-track-subgrade dynamic performance with crumb rubber in ballast layer

Guo, Yunlong; Shi, Can; Zhao, Chunfa; Markine, Valeri; Jing, Guoqing

DOI
10.1016/j.conbuildmat.2022.127559

Publication date
2022

Document Version
Final published version

Published in
Construction and Building Materials

Construction and Building Materials 336 (2022) 127559

Contents lists available at ScienceDirect

Construction and Building Materials

journal homepage: www.elsevier.com/locate/conbuildmat

Numerical analysis of train-track-subgrade dynamic performance with crumb rubber in ballast layer

Yunlong Guo [a], Can Shi [b,c], Chunfa Zhao [b,*], Valeri Markine [a], Guoqing Jing [d]

[a] Faculty of Civil Engineering and Geosciences, Delft University of Technology, Delft 2628CN, Netherlands
[b] Train and Track Research Institute, National Traction Power Laboratory, Southwest Jiaotong University, Chengdu 610031, China
[c] College of Civil and Transportation Engineering, Shenzhen University, Shenzhen 518060, China
[d] School of Civil Engineering, Beijing Jiaotong University, Beijing 100044, China

ARTICLE INFO

Keywords:
Discrete element method
Finite difference method
Ballast
CR
Crumb rubber
Tire-derived aggregate
Multibody dynamics

ABSTRACT

Crumb rubber (CR) has been proposed to apply in the ballast or sub-ballast layer for ballast degradation mitigation and vibration (noise) reduction. The CR can change the ballast layer stiffness, which can affect the train-track-subgrade dynamic performance and cause travel comfort and safety issues. Towards this, this study aims at confirming 1) how much the CR application can affect the dynamic performance of train and ballast layer; 2) to what extent the CR-ballast layer can distribute the train loadings to reduce subgrade surface stress.

To achieve this aim, a whole train-track-subgrade system model was built by coupling multibody dynamics (MD), discrete element method (DEM) and finite difference method (FDM). The MD was used to build the train, including one vehicle body, two bogies and four wheelsets. The DEM was used to build the ballasted track, including rail, sleepers and ballast layer. The FDM was used to build the subgrade. Using the coupled model, the dynamic performance of train and track were studied, including the vehicle body acceleration, wheel-rail force, rail dynamical bending moment, sleeper acceleration, sleeper displacement and ballast acceleration. In addition, the energy dissipation of the ballast bed was also presented. For the subgrade, the subgrade surface acceleration and surface stress were measured and analysed. In the model, different CR size and percentage were considered.

Results show that using the CR in ballast layer can increase the accelerations of sleeper, rail and train. But it can decrease the ballast degradation, subgrade surface acceleration and subgrade surface stress. CR helps consume train loading energy, reducing the energy that has to be consumed by ballast friction. Small size CR (8–22.4 mm) has greater influence on dynamic performance of the whole train-track-subgrade system than big size CR (9.5–63 mm). In summary, 10% percentage of CR-ballast mixture is recommended, and for CR size it is difficult to give a recommendation. Small size CR increase ballast acceleration more than big size CR, but small size CR are better at improving sleeper displacement, subgrade stress and ballast bed stress.

1. Introduction

Railways in all sectors, including urban light rail railway, high speed railway, heavy haul, intercity and metro, play a significant role in the transportation system worldwide [1]. Ballasted track, as the most widely-used type, consists of rails, fasteners, sleepers and ballast layer. It is most widely-used for reasons of low construction cost, simplicity in design and construction, as well as easy maintenance [4].

The ballast layer, a crucial component of ballast track, provides resistances to sleepers, transmits and distributes the loadings or impacts from the sleepers to the subgrade, as well as provides rapid drainage [5]. Generally, it is composed of blasted (quarried) rock aggregates, which conform to certain characteristics such as narrow-graded (20 mm-60 mm), particle size and shape, surface roughness, particle and bulk density, hardness, toughness, free of dust, resistance to attrition and weathering and so on [6].

Even though various standards and specifications have been made for ballast [6,9,10], under the repeated loading and environmental conditions, it gradually deteriorates and becomes fouled by the fine particles from external or ballast breakage and abrasion (wear/attrition) [11,12]. Deteriorated ballast bed, which is filled with fouling material, cannot provide enough shear strength and hydraulic conductivity, causing the instability of track [13,14]. More importantly, the increasing train speed and freight capacity exacerbates its degradation, leading to

* Corresponding author.
E-mail address: cfzhao@swjtu.edu.cn (C. Zhao).

https://doi.org/10.1016/j.conbuildmat.2022.127559
Received 3 February 2022; Received in revised form 8 March 2022; Accepted 16 April 2022
Available online 29 April 2022

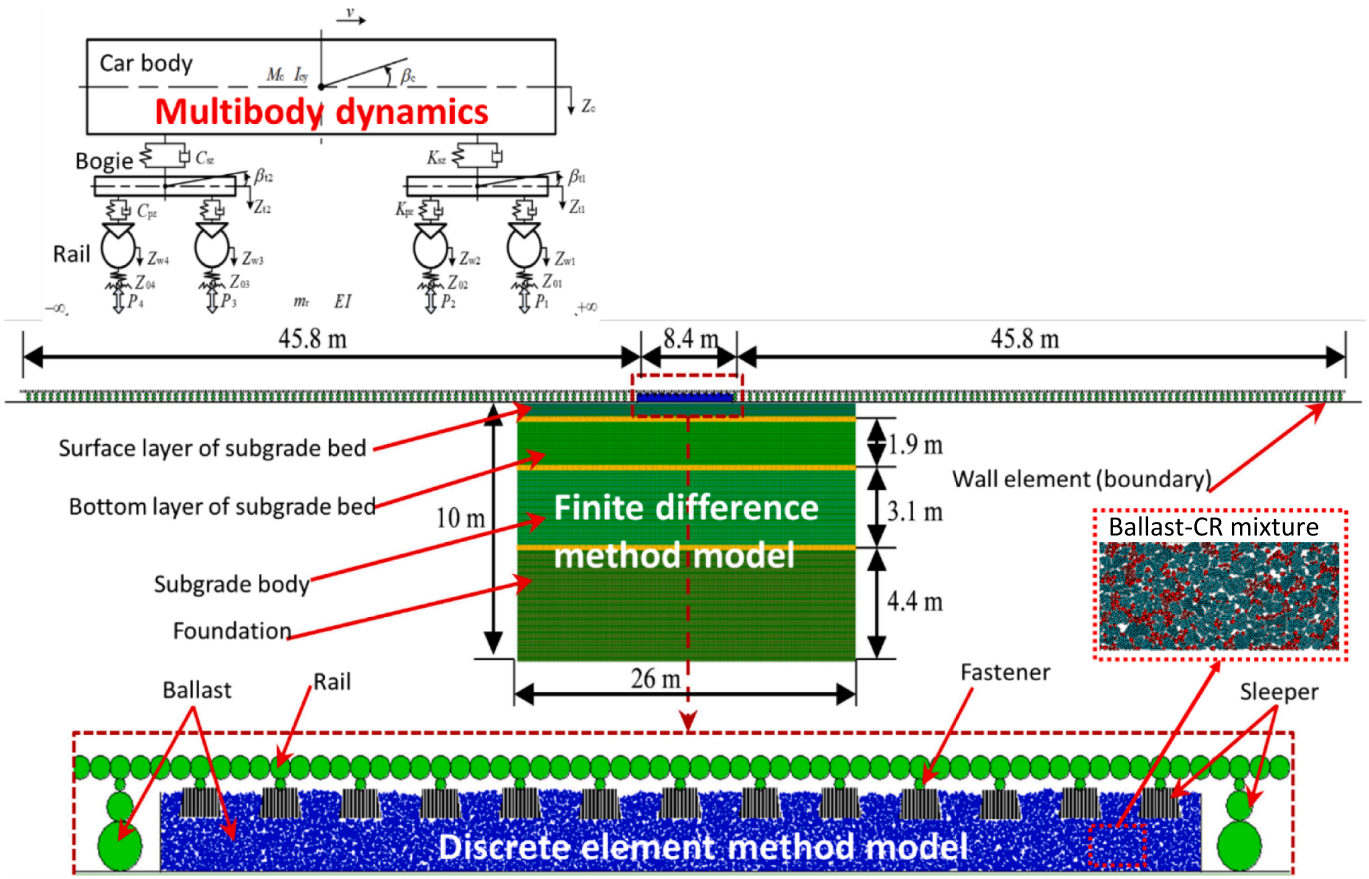

Fig. 1. Coupled multibody dynamics, finite difference method and discrete element method model.

the unacceptable track deformation and frequent maintenance [15,16].

Therefore, it is crucial to mitigate ballast degradation, prolonging the service life of ballast track. In recent decades, various kinds of techniques have been proposed, such as under sleeper pads, under ballast mat, geogrid, and polyurethane [17–21]. Although it has been demonstrated that these techniques can alleviate ballast degradation, there still exists some limitations. Among them, the most important one is the higher construction costs [22]. In addition, the maintenance may also be affected, such as tamping and stone blowing.

In response to the limitations, the solution of mixing crumb rubber (which is also named as tire-derived aggregates in some studies) with ballast particles has been proposed, for the advantages that it is economic and environmental-friendly. The CR is made of shredded waste tire, and it has been proved that mixing the CR with ballast is an effective means for ballast degradation and noise reduction.

To be more specific, the idea of using CR was first proposed in [23] for reducing vibration and noise transmitted from railway to nearby buildings, however, the CR was added in the foundation. After that, it was studied the characterisation and the vibration alleviation of the sub-ballast mixed with the CR [24–26]. In addition, mixing the CR, steel furnace slag and coal wash as sub-ballast layer was studied with cyclic triaxial test to confirm optimal CR percentage (10%) and the mixture energy-absorbing capacity [27].

For the ballast layer, the CR was utilised in ballast layer as elastic particles to reduce ballast degradation in [28]. Afterwards, more laboratory tests, including direct shear test and ballast box test, were conducted to confirm the optimal CR percentage as 10% in [22]. In [29] the DEM model of direct shear test was applied to study the contact forces of ballast-CR mixture, which proves the ballast breakage was alleviated through reducing larger contact forces (over 250 kN). Afterwards, the CR was applied in the field track [30] as well as the track in some special areas, such as the bridge and desert area [31,32], and the dynamic performance of ballast layer was studied with impact loading tests or cyclic loading tests. Particularly, in [13], the drainage of ballast-CR mixture was studied, and the factors were considered, including the CR size and percentage. This study proved that less than 30% percentage CR (by volume) can still have acceptable drainage.

According to the earlier studies, it can be concluded that the CR is possible to apply in ballast layer, nevertheless, there are still some non-negligible research gaps before applying the CR in the field. Specifically, all the earlier tests focused on gross and global performances of ballast-CR mixture, and most of the studies applied experimental laboratory tests. The global performances include settlement, shear strength, ballast degradation (evaluated by gradation change) and drainage, while the laboratory tests were direct shear test, Los Angeles abrasion test and ballast box test. This can demonstrate that the research gaps are 1) limited studies have been performed on the performance of full-scale track with the CR, 2) most studies only focused on ballast-CR performance and ignored positive influence on subgrade (e.g. stress reduction), 3) few studies present the ballast-CR dynamic performance from particle level with numerical simulations (e.g. energy dissipation, contact forces) and 4) most importantly, no studies have been found on whether the CR affects the wheel-rail interaction and vehicle dynamic behaviour, and this possibly happens due to the reduced stiffness of ballast-CR bed.

In response to these research gaps, a coupled model was applied to study the vehicle dynamic behaviour, wheel-rail interaction and ballast-CR dynamic performances when applied the CR in ballast layer with the presence of subgrade. The coupled model is made of three parts that are simulated by different numerical simulation method. Specifically, vehicle (car body, bogies and wheels) was simulated with the multibody dynamics, ballasted track (rail, fasteners sleeps and ballast particles)

Table 1
Notations in the VTCD model (modified after [36]).

M_c	Mass of car body	K_{pz}	Primary suspension stiffness
M_t	Mass of bogie	K_{sz}	Secondary suspension stiffness
M_w	Mass of wheelset	C_{pz}	Primary suspension damping
J_c	Inertia of car body	C_{sz}	Secondary suspension damping
J_t	Inertia of bogie	$\beta_{i(t)}$	Pitching angular displacement
$Z_{w(t)}$	Displacement of component	$Z_{oi(t)}$	Irregularity function
$P_{i(t)}$	Wheel/rail contact force		

Table 2
Vehicle parameters of multibody dynamics model (parameters verified in [37–39]).

Parameter	Value	Parameter	Value
Mass of car body	61927 kg	Primary suspension stiffness	2.123×10^6 N/m
Mass of bogie	7840 kg	Secondary suspension stiffness	1.67×10^6 N/m
Mass of wheelset	5430 kg	Primary suspension damping	2.5×10^4 N·s/m
Inertia of car body	1.443×10^6 kg·m^2	Secondary suspension damping	1.0×10^5 N·s/m
Inertia of bogie	1.311×10^3 kg·m^2	Semi-longitudinal distance between bogies	4.5 m
Wheel radius	0.43 m	Semi-longitudinal distance between wheelsets in a bogie	1.4 *m*
Train type (brand)	Heavy haul (Chinese HXD1)	Vehicle speed	80 km/h

Table 3
Parameters for discrete element method track model (modified after [39]).

Parameters	Value	Parameters	Value
Rail disc radius	75 mm	Sleeper disc radius	5 mm
Rail disc density	490 kg/m^3	Sleeper disc contact normal stiffness	1×10^9 N/m
Rail disc contact normal stiffness	1.05×10^{10} N/m	Sleeper disc contact shear stiffness	1×10^9 N/m
Rail disc contact shear stiffness	1.05×10^{10} N/m	Sleeper disc friction	0.7
Rail parallel bond radius	37.27 mm	Ballast disc density	2600 kg/m^3
Rail parallel bond radius multiplier	0.497	Ballast disc radius	4
Rail parallel bond normal stiffness	1.427×10^{12} N/m^3	Ballast disc contact normal stiffness	3×10^8 N/m
Rail parallel bond shear stiffness	5.5297×10^{11} N/m^3	Ballast disc contact shear stiffness	3×10^8 N/m
Fastener disc density	2500 kg/m^3	Ballast disc friction	0.7
Fastener disc radius	20 mm	Ballast parallel bond normal stiffness	1×10^{10} N/m
Fastener disc contact normal stiffness	1×10^8 N/m	Ballast parallel bond shear stiffness	1×10^{10} N/m
Fastener disc contact shear stiffness	1×10^8 N/m	Wall contact normal stiffness	3×10^8 N/m
Sleeper disc density	3129 kg/m^3	Wall contact shear stiffness	3×10^8 N/m

was simulated with the discrete element method (DEM), and subgrade is simulated with the finite difference method (FDM). With this coupled model, results were obtained including vehicle body acceleration, wheel-rail force, rail dynamical bending moment, sleeper acceleration, sleeper displacement and ballast acceleration. The energy dissipation of ballast bed was also presented. For the subgrade, the subgrade surface acceleration and surface stress were calculated and analysed. By analysing these results, advices can be given from the influence of CR on the whole system (vehicle-track-subgrade). Moreover, the coupled model is a new effective tool for future ballast-related problems.

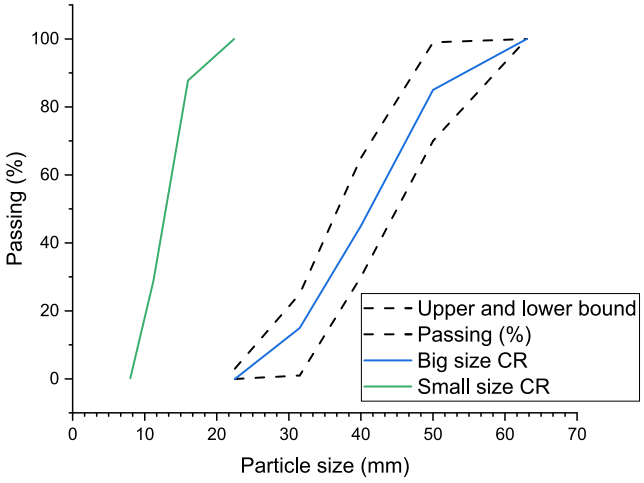

Fig. 2. Particle size distributions of big-size and small-size crumb rubber.

Table 4
Parameters of finite difference method subgrade model (modified after [39]).

Track components	Poisson's ratio	Young modulus (MPa)	Density (kg/m3)
Surface layer of subgrade bed	0.25	180	1950
Bottom layer of subgrade bed	0.25	110	1900
Subgrade body	0.3	80	1800
Foundation	0.3	60	1700

2. Methodology

2.1. Model description

As shown in Fig. 1, the main methodology is using a coupled model to study the dynamic behaviour of vehicle, ballast-CR dynamic performances and subgrade dynamic responses.

The multibody dynamics model was a theoretical model developed by Wanming Zhai [33], the DEM model was built with the software particle flow code (PFC) and the FDM model was built with the software Fast Lagrangian Analysis of Continua (FLAC).

2.1.1. Multibody dynamics model

The classic model of multibody dynamics developed by Zhai [33] (Vehicle-Track Coupled Dynamics: VTCD) was applied in this study to build the vehicle including car body, bogies and wheels, as shown in Fig. 1. The multibody dynamics model has been used to calculate the wheel-rail forces, vehicle acceleration, rail acceleration and ballast layer acceleration [34,35]. It can predict the dynamic performance of the whole system of normal track with ballast layer simplified as mass blocks. The notations of the VTCD model are given in Table 1.

For the vehicle part, all the components (car body, bogie and wheel) are regarded as rigid bodies, and they are connected by a damper and spring. The vehicle rigid system has ten degrees of freedom, and the vehicle parameters used in the model are given in Table 2. In the table, the primary suspension is the dampers and springs between wheels and bogies, while the secondary suspension is the dampers and springs between bogies and car body (Fig. 1).

2.1.2. Discrete element method model

Some inevitable conditions that result from discrete nature of ballast assemblies cannot be considered in the multibody dynamics model, such as hanging sleeper, ballast bed stiffness non-uniformity and ballast pocket. These factors have great influence on the wheel-rail forces,

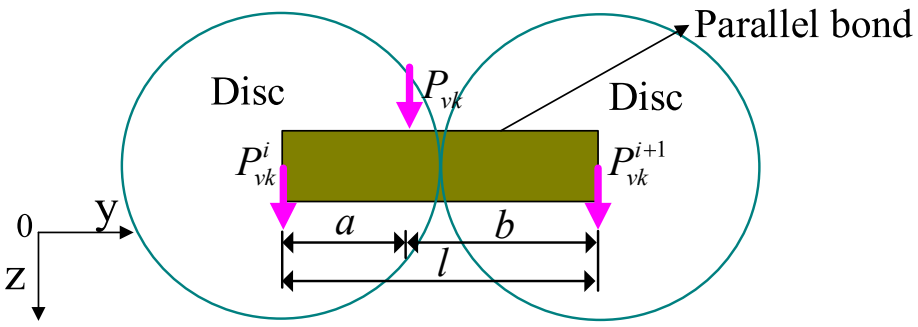

Fig. 3. Conversion method of wheel-rail contact force.

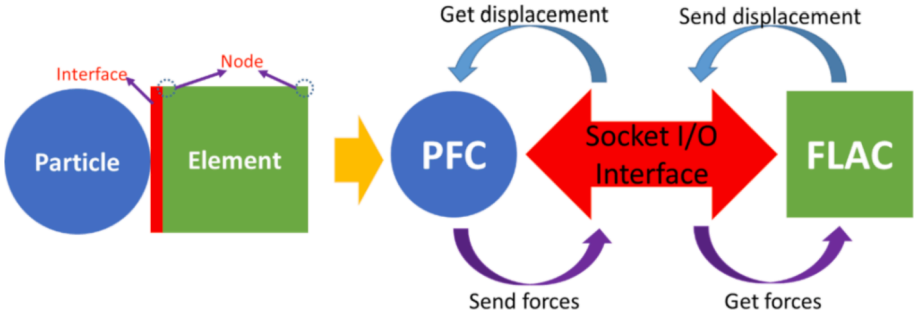

Fig. 4. Coupling procedure of discrete element method and finite difference method.

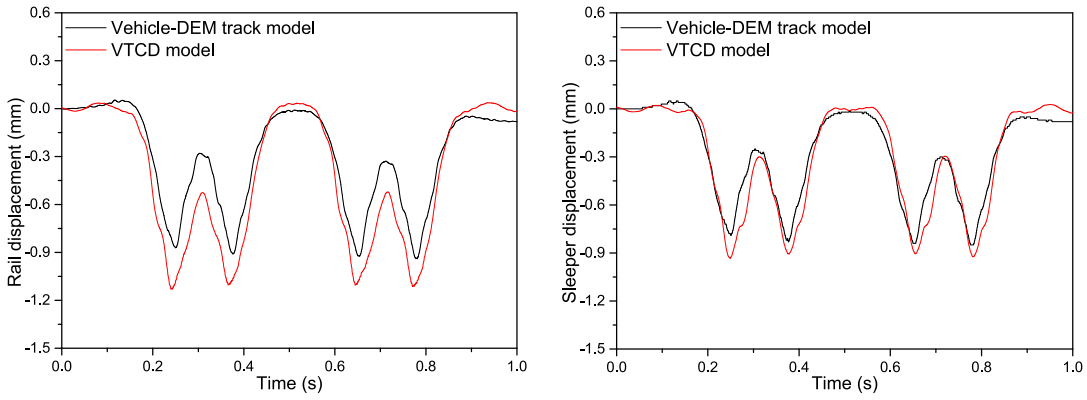

Fig. 5. Two models' comparison results on rail displacements and sleeper displacements.

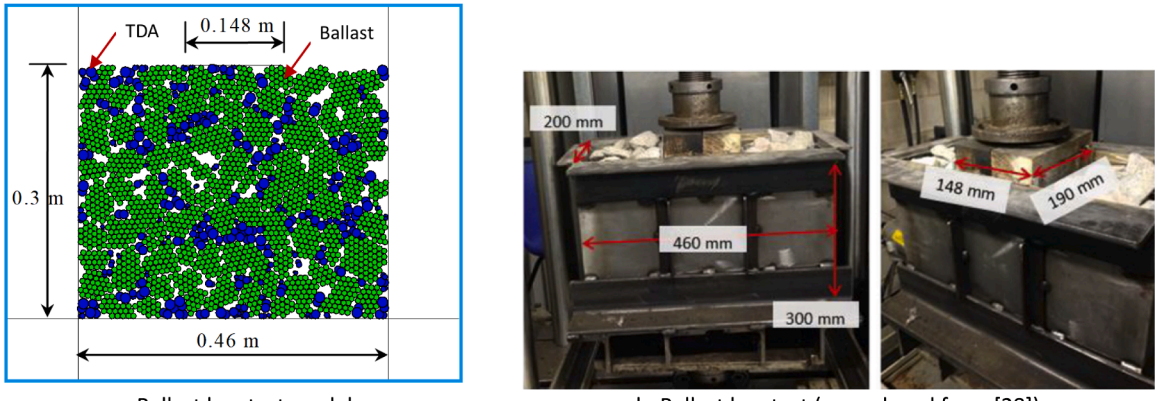

a. Ballast box test model

b. Ballast box test (reproduced from [28])

Fig. 6. Ballast box test model and ballast box test performed in [28].

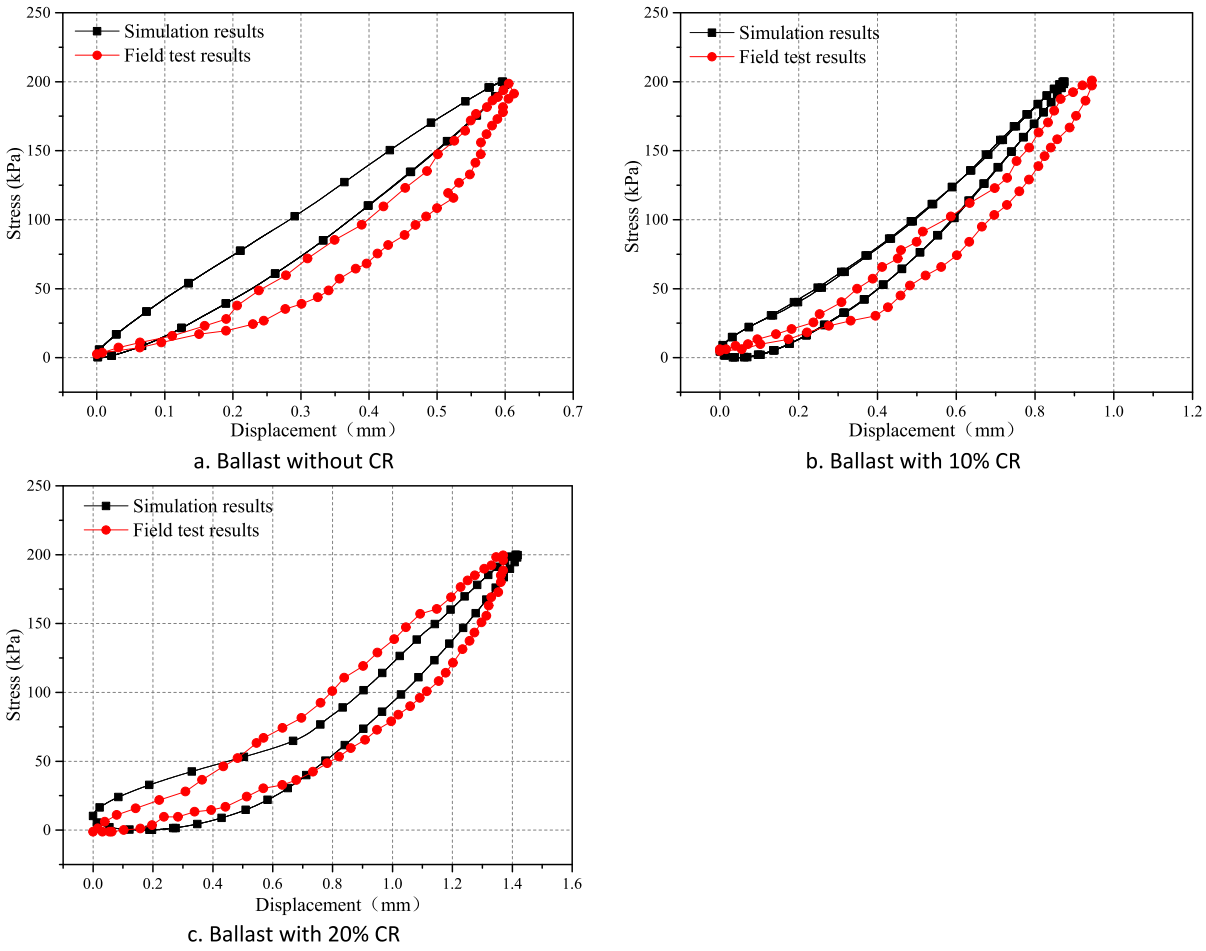

Fig. 7. Comparison ballast box test results of DEM simulations and experiments.

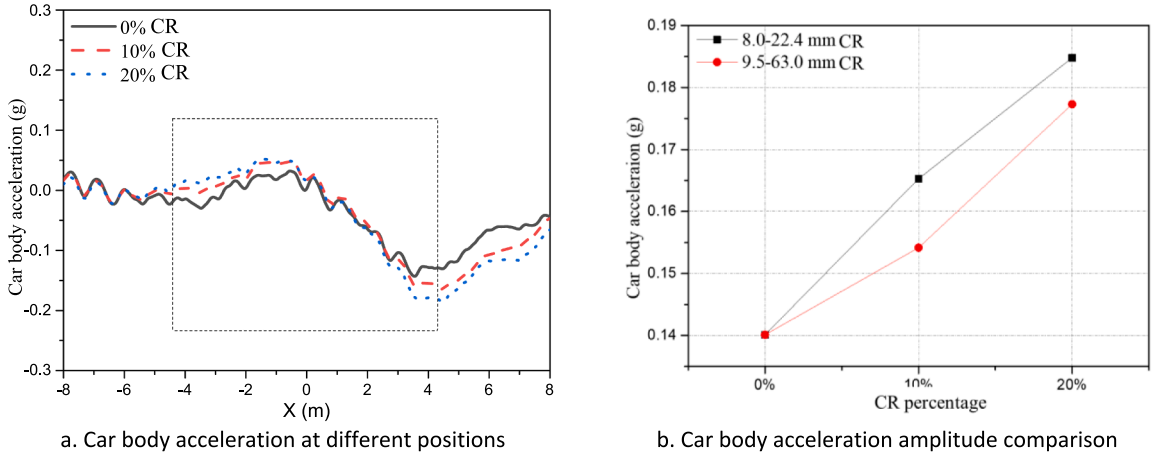

Fig. 8. Car body acceleration operating on ballasted track with CR.

causing big error or even false results. For this, the track part was built with the DEM model considering that the ballast-CR mixture has irregular movements and dynamic responses to cyclic loadings.

The DEM was introduced by Cundall [40] and has been used for studies on the mechanical behaviour of ballast particles by many researchers [18,41–44]. It provides a better insight into the mechanical behaviour and dynamic performance of ballast particles both microscopically and macroscopically [45,46]. It also has the advantage that one sample can be used for various loading conditions [39,47,48]. In addition, some features that cannot be examined experimentally can be studied, for instance, particle movements, inter-particle friction, particle breakage and distribution of contact force chains [12,50–52].

As shown in Fig. 1, in the coupled model, the track model was built with the DEM, including rail, fasteners, sleepers and ballast particles. To save the computation costs, the track model was built as 100 m long with two types of ballast layers, and it was built long enough to couple the vehicle model. One type of ballast layer was 8.4 m long at the middle, and it was built with irregular shapes of ballast particles, Clusters

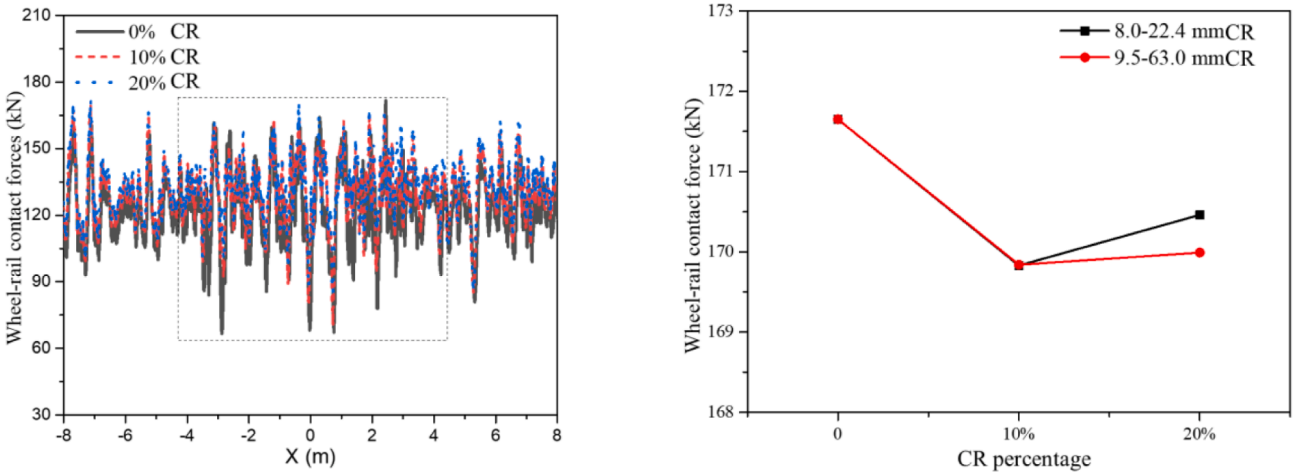

a. Wheel-rail contact forces at different positions

b. Maximum wheel-rail contact force

Fig. 9. Wheel-rail contact force operating on ballasted track with CR.

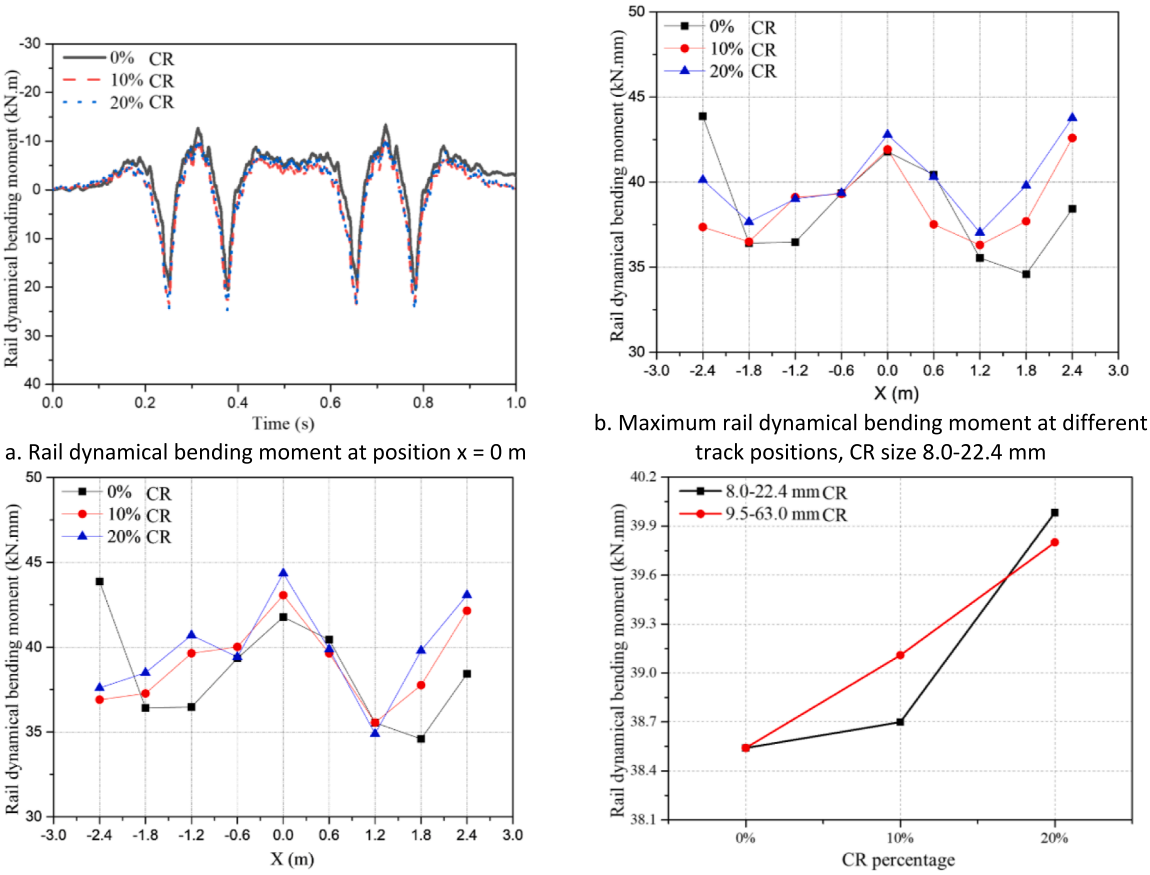

a. Rail dynamical bending moment at position x = 0 m

b. Maximum rail dynamical bending moment at different track positions, CR size 8.0-22.4 mm

c. Maximum rail dynamical bending moment at different track positions, CR size 9.5-63.0 mm

d. Average value of maximum rail dynamical bending moments of different CR percentages

Fig. 10. Rail dynamical bending condition of ballasted track with CR.

(clusters explained in [46]). The other type of ballast layer had two sections at two sides with the length at 45.8 m each, and they were built with ballast particles simplified as discs.

In addition, each sleeper at the two sections were also built as one disc, and each sleeper was bonded to one disc that presents ballast particles. The track in the middle (8.4 m) included 13 sleepers, and the irregular ballast particles in the middle section were built according the British standard gradation [53]. The rail was built as beam with bonded discs (parallel bond), and a fastener was built as a disc. The fastener was bonded to the sleeper and rail. The sleeper was built with the Clump, which is an assembly of discs. The parameters for the DEM track model are given in Table 3. More details about this DEM model can be found in [39].

In the DEM mode, the ballast particles were supported by wall

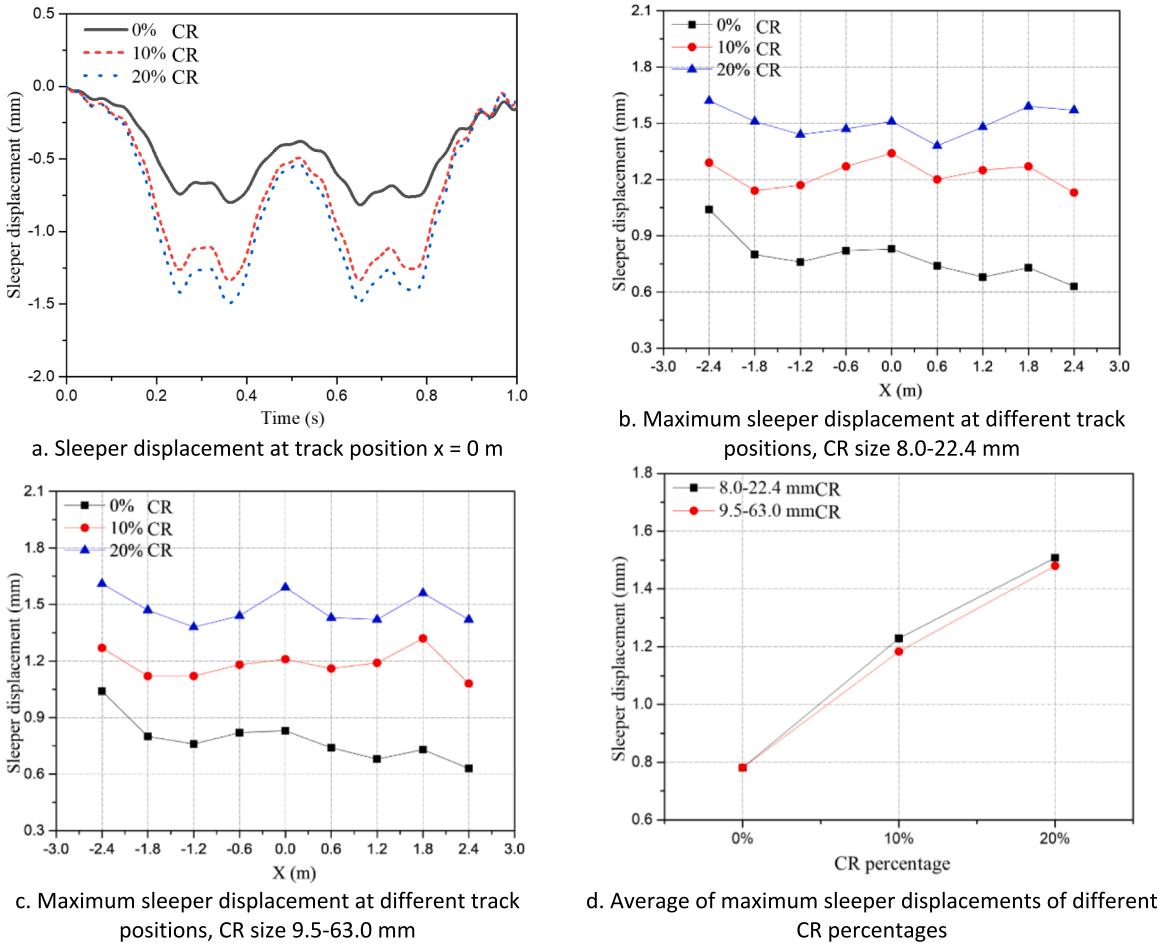

a. Sleeper displacement at track position x = 0 m

b. Maximum sleeper displacement at different track positions, CR size 8.0-22.4 mm

c. Maximum sleeper displacement at different track positions, CR size 9.5-63.0 mm

d. Average of maximum sleeper displacements of different CR percentages

Fig. 11. Sleeper displacement of ballasted track with CR.

elements with the stiffness as 8×10^7 kN/m, and these wall elements were used for interactions between the DEM model (track) and FDM model (subgrade). This will be explained more specifically in Section 2.1.5.

The ballast bed was made of the mixture of ballast particles and CR. Two types of CR particle size ranges (8.0–22.4 and 9.5–63.0 mm) were compared in this study with the percentages at 0, 10 and 20% (by weight), respectively. The ballast-CR mixture is at the condition of CR size at 8.0–22.4 mm, 20% percentage. The particle size distributions (PSDs) of the two kinds of CR are shown in Fig. 2. In the figure, the upper and lower bound is the PSD requirement for railway ballast in British standard [53].

2.1.3. *Finite difference method*

The subgrade (including part of foundation) was built with the FDM software, FLAC, Fast Lagrangian Analysis of Continua. The FLAC is numerical simulation software that was developed for cutting-edge analysis of discrete materials, such as soil and rock considering water. This calculation method came from hydromechanics initially, and it was used to study every fluid particle changes with time, including particle movements, velocity and pressure.

The FLAC has also been used for solid mechanics by generating meshes, and treating the nodes as fluid particles. It has been applied for soil analysis in many earlier studies [39,54–56]. It was applied for soil engineering (e.g. tunnel, subgrade and foundation) that needs continuum analysis, and compared with other continuum method it can simulate conditions with big displacements and strains.

In addition, the FLAC was applied in this study due to it has higher efficiency than with the DEM at simulating the subgrade. Because, subgrade is made of huge amounts of soil particles. Particularly, the subgrade is fully compacted and can be treated as continuum material.

As shown in Fig. 1, the length of the subgrade was built as 26 m and depth was 10 m. Lengths of different layers were marked in the figure. The subgrade length was longer than the ballast track (in the middle), because the force or stress distribution in subgrade is a shape of pyramid.

The instantaneous dynamic performance of subgrade was focused in this study, including the subgrade surface acceleration and surface stress. Obvious subgrade deformation usually occurs after long-term train cyclic loadings (e.g., millions of loading cycles), which means we can ignore the long-term deformation influence on subgrade surface acceleration and surface stress under a few cyclic loading. For this condition, isotropic and linear-elastic constitutive model was applied to build the four layers with different parameters, as shown in Table 4. In other words, this model simplified the subgrade, because we consider the short-term subgrade performance. More explanations about the FDM subgrade model can be found in [39].

2.1.4. *Coupling multibody dynamics model with discrete element method model*

The multibody dynamics vehicle model was coupled with DEM track model through the interaction between wheel and rail. To be more specific, the wheel-rail contact forces from vehicle were firstly acted on the rail, and the rail displacements were obtained. With the rail displacements, the wheel-rail contact forces were recalculated and then applied to the vehicle. Using this method, the real-time coupling of these two models were achieved.

The Hertz non-linear contact theory was used to calculate vertical wheel-rail contact forces. As shown in Equation (1), for the *i*th wheel,

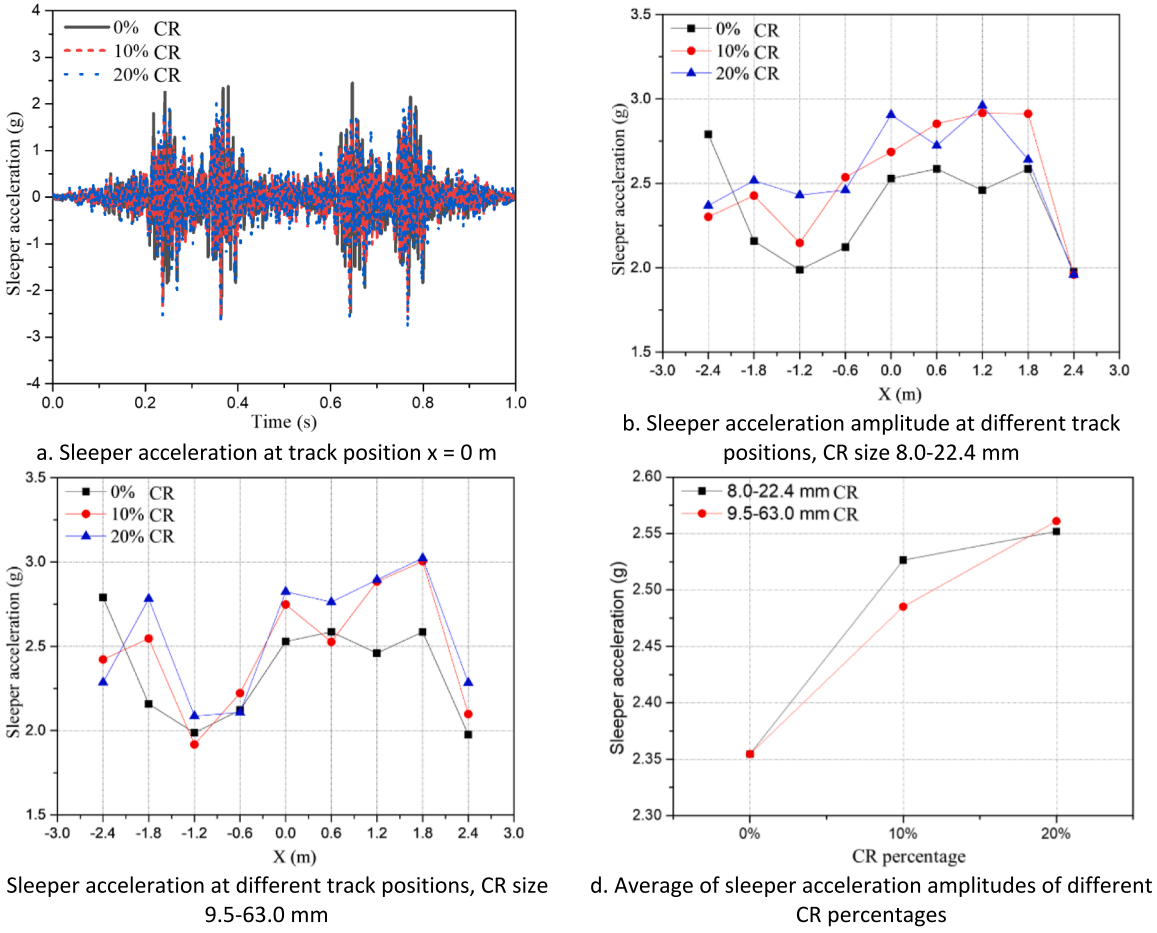

a. Sleeper acceleration at track position x = 0 m

b. Sleeper acceleration amplitude at different track positions, CR size 8.0-22.4 mm

c. Sleeper acceleration at different track positions, CR size 9.5-63.0 mm

d. Average of sleeper acceleration amplitudes of different CR percentages

Fig. 12. Sleeper acceleration of ballasted track with CR.

the contact force, $P_{i(t)}$, is calculated through the elastic compressive deformation$\delta Z(t)$. G is a constant of wheel-rail contact with the value of $3.86R^{-0.115} \times 10^{-8}$ in this study [33].

$$p_i(t) = \left[\frac{1}{G}\delta Z(t)\right]^{\frac{3}{2}} \tag{1}$$

The wheel-rail contact force calculation method treats the rail as a beam of Bernoulli-Euler or Timoshenko, which is different from the DEM rail made by discrete discs. In DEM models, forces can only be applied at the disc centre, while it is not correct to assume that the wheel-rail contact are always right above the disc centre. To solve this problem, a conversion method of wheel-rail contact force was developed.

As shown in Fig. 3, the conversion method is transforming the force (P_{vk}) to the centres of two adjacent discs (P_{vk}^{i} and P_{vk}^{i+1}) with the Eq. (2). In the conversion method, the rail is essentially equivalent to a beam with rectangular cross-section. Eq. (2) is according to the principle of statistical equilibrium of simply supported beam. In the equation, l is the distance between the two adjacent discs, while a and b are the distance between wheel-rail contact point and the two adjacent discs, respectively (Fig. 3).

$$P_{vk}^{i} = \frac{P_{vk}b^2(l+2a)}{l} \tag{2a}$$

$$P_{vk}^{i+1} = \frac{P_{vk}a^2(l+2b)}{l} \tag{2b}$$

2.1.5. Coupling discrete element method model with finite difference method model

The PFC and FLAC are two kinds of software developed by ITASCA, and the coupling the two types of software has been achieved easily through the function of Socket I/O (input/output). The coupling method was introduced in details in [39,57], and briefly explained as follows.

The coupling principle is generating many walls between the PFC and FLAC to transmit data, including force, velocity and displacement. The walls have the same size as the mesh size of the FLAC model (subgrade). Firstly, the loading from sleeper was transmitted to the ballast particles, and according to the Force-displacement discipline, the contact forces (at the interface) between the walls and ballast particles can be obtained. The contact forces at the interface were applied to the mesh nodes. The whole coupling procedure is shown in Fig. 4.

2.2. Model calibration and validation

The multibody dynamics vehicle model has been calibrated and validated in many studies [33,34,58]. The DEM track model was calibrated and validated in the reference [39] using experimental and field tests (direct shear test, rail acceleration, sleeper acceleration and ballast acceleration), including the particle shape (based on ballast images) and model parameters (rail, fastener and sleeper). The FDM subgrade model and coupling the DEM/FDM models were confirmed to be correct by field tests in [39] as well.

Two aspects are explained in this section, including 1) the validation of coupling multibody dynamic model and DEM model, and 2) the validation and calibration of the DEM ballast layer model with the CR.

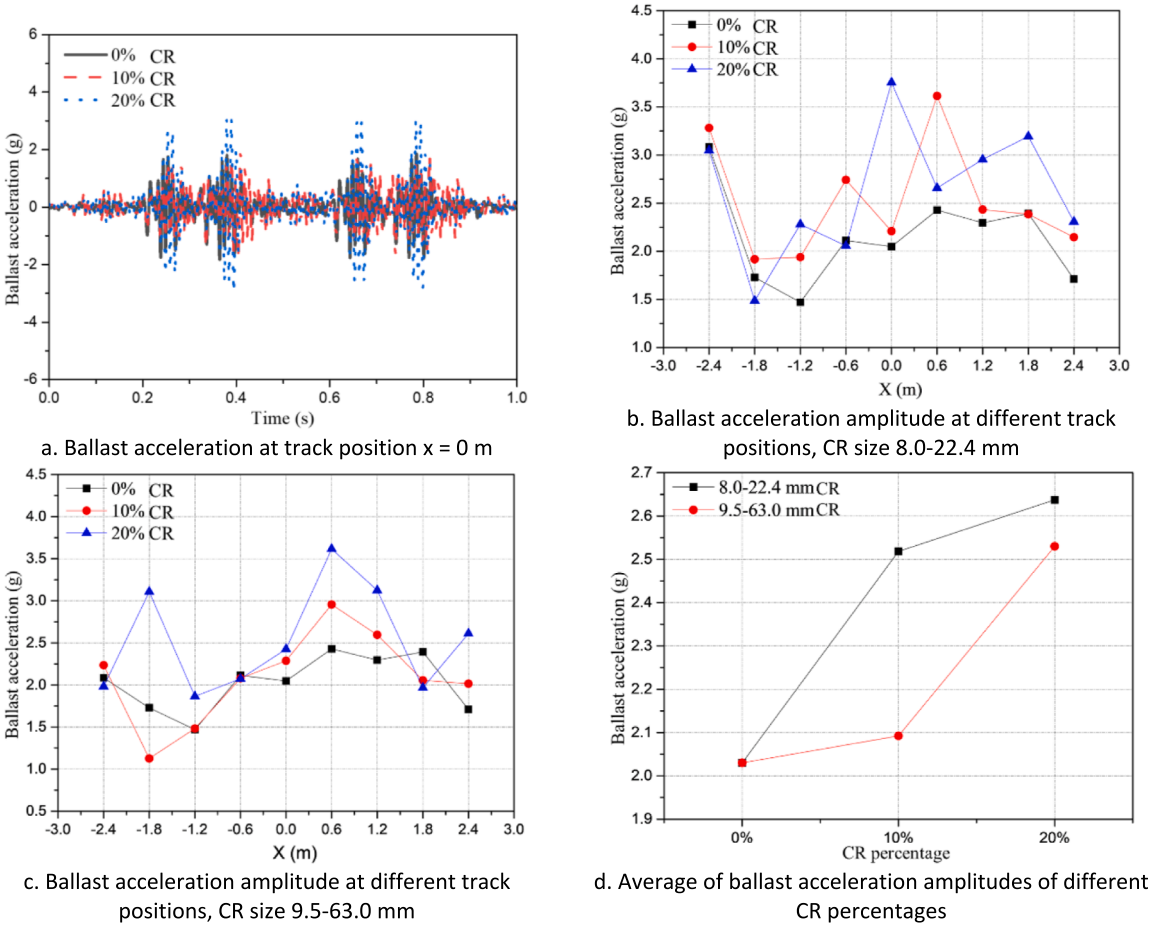

a. Ballast acceleration at track position x = 0 m

b. Ballast acceleration amplitude at different track positions, CR size 8.0-22.4 mm

c. Ballast acceleration amplitude at different track positions, CR size 9.5-63.0 mm

d. Average of ballast acceleration amplitudes of different CR percentages

Fig. 13. Ballast acceleration of ballasted track with CR.

2.2.1. Validation of coupling multibody dynamics model and DEM model

The coupling of vehicle and ballasted track models was validated by comparing the results (obtained from the coupled models) to results obtained from VTCD. The results include wheel-rail contact forces, rail displacements, rail accelerations, sleeper displacements and sleeper accelerations.

The vehicle parts of the two models were the same, but their track parts were different. The coupled models applied the DEM ballasted track model, while the VTCD applied the mass blocks to simulate ballast layer. The vehicle speed was 80 km/h.

The comparison results can be found in [38]. The results of two models are very similar at the tendency and magnitude, and they can almost fit to each other. An example was given in Fig. 5. After comparing the results from the two models, it was confirmed that the coupled models can be used for further analysis.

2.2.2. Calibration and validation for DEM model with CR

The CR parameters and the ballast-CR mixture model were calibrated and validated by comparing the ballast box test results in the reference [28]. According to the test rig configuration in [28], a ballast box model was built as shown in Fig. 6 [57].

As shown in Fig. 7, the force–displacement curves are almost matched under the pressure at 200 kPa. The experimental tests and DEM simulation both applied the CR size at 8.0–22.4 mm. From the figure, simulation results show that the CR percentages at 0, 10 and 20% have the maximum displacement at 0.6, 0.9 and 1.4 mm, which are almost the same as experimental results [57]. This means in the model the parameters of CR (shear and normal stiffnesses) is reasonable as 2×10^7 N/m.

3. Results and discussions

3.1. Vehicle dynamic performance

3.1.1. Car body acceleration

Fig. 8a summaries car body accelerations when operating at different track positions. In the figure, the abscissa axis presents the track positions. Specifically, the middle of the DEM track model is 0, and section from −4.2 to 4.2 has the ballast-CR mixture in track model. The CR size in Fig. 8a is 8.0–22.4 mm. From Fig. 8a, it can be observed that the car body accelerations of 0, 10 and 20% CR have similar trends, but with different amplitudes. To be more specific, car body acceleration amplitude without CR is 0.14 g, and with the CR the amplitudes increase to 0.16 g (10% CR) and 0.18 g (20%), respectively.

Fig. 8b summaries all the car body acceleration amplitudes on different conditions of CR percentage or size ranges. From the figure, it can be seen that the car body acceleration amplitude increases as the CR percentage increases. For the 8.0–22.4 mm CR, the amplitudes increase by 18% as CR percentage increases from 0 to 10%, while from 10 to 20% the amplitudes increase 14%. For the 9.5–63.0 mm CR, the amplitudes increase by 10% as CR percentage increases from 0 to 10%, while from 10 to 20% the amplitudes increase 17%. Moreover, the figure demonstrates that small size CR (8.0–22.4 mm) has greater influence on the acceleration amplitude than large size (9.5–63.0 mm).

The accelerations were increased by the CR, but the increment is less than 0.5 m/s^2. This means the maximum acceleration is 0.18 g that is still smaller than the stipulated limits (2.5 m/s^2) in Chinese standards.

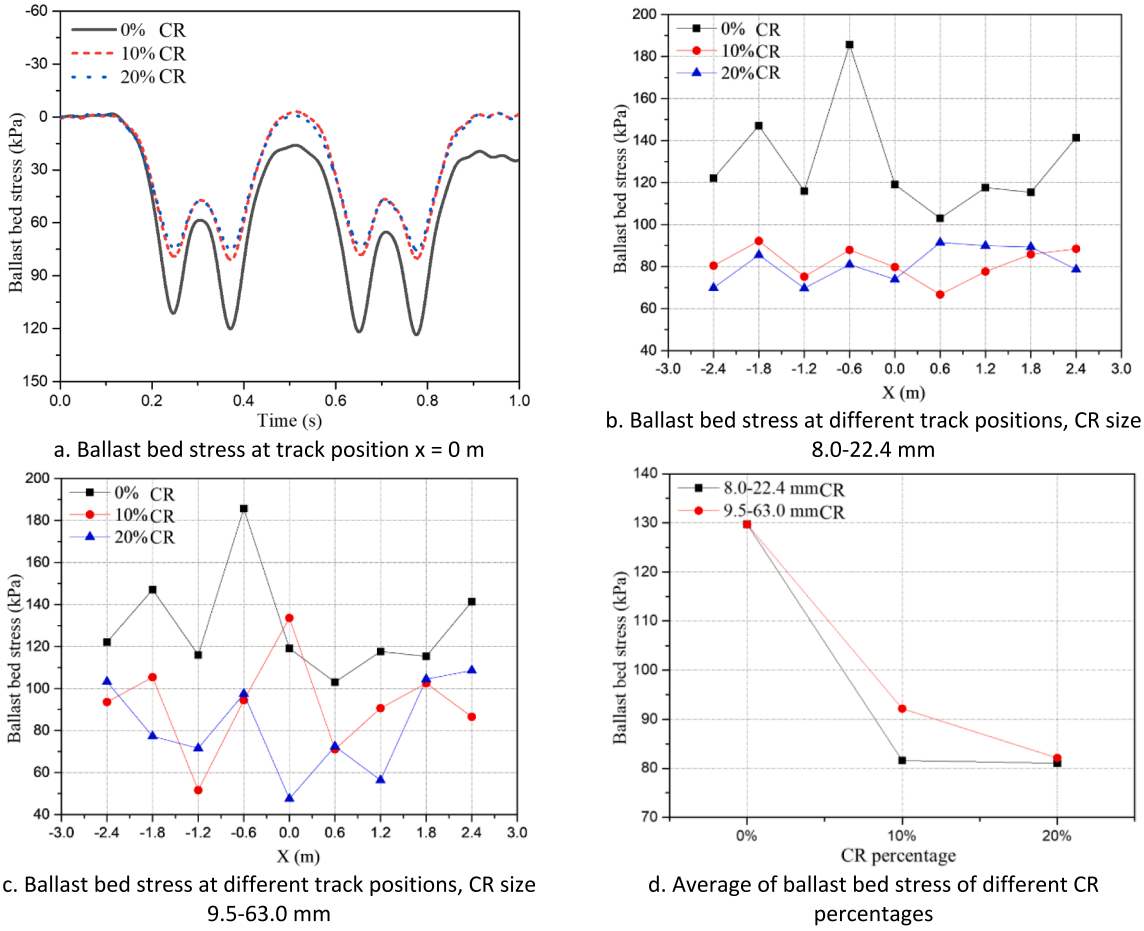

a. Ballast bed stress at track position x = 0 m

b. Ballast bed stress at different track positions, CR size 8.0-22.4 mm

c. Ballast bed stress at different track positions, CR size 9.5-63.0 mm

d. Average of ballast bed stress of different CR percentages

Fig. 14. Ballast bed stress of ballasted track with CR.

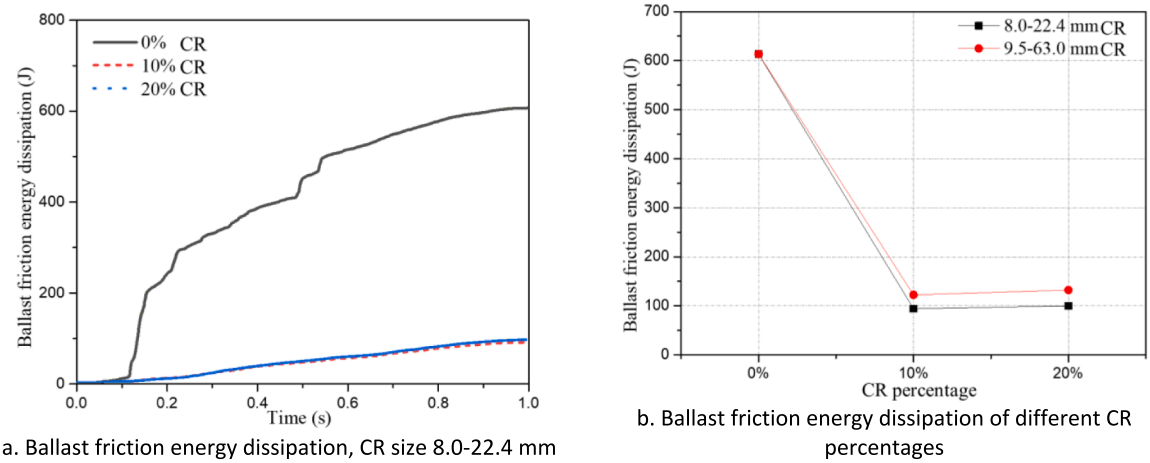

a. Ballast friction energy dissipation, CR size 8.0-22.4 mm

b. Ballast friction energy dissipation of different CR percentages

Fig. 15. Ballast friction energy dissipation of ballasted track with CR.

3.1.2. *Wheel-rail contact force*

Fig. 9a summaries the wheel-rail contact forces of the first wheelset when vehicle was operating at different track positions. The figure shows that the peak and valley points are almost at the same track positions but with different magnitudes. Specifically, the maximum wheel-rail contact force without CR is 171.7 kN, while the forces slightly reduce to 169.8 kN (10% CR) and 170.5 (20% CR), respectively.

Fig. 9b presents the maximum wheel-rail contact forces on different conditions of CR percentage and size. The figure shows that the CR can slightly reduce the wheel-rail contact forces, but it can be ignored due to the change is within 1%. This means the CR has few influences on the wheel-rail contact.

3.2. *Ballasted track dynamic performance*

3.2.1. *Rail dynamical bending moment*

Rail dynamical bending moment can present the rail bearing condition. As shown in Fig. 10a, the rail dynamical bending moments (x = 0

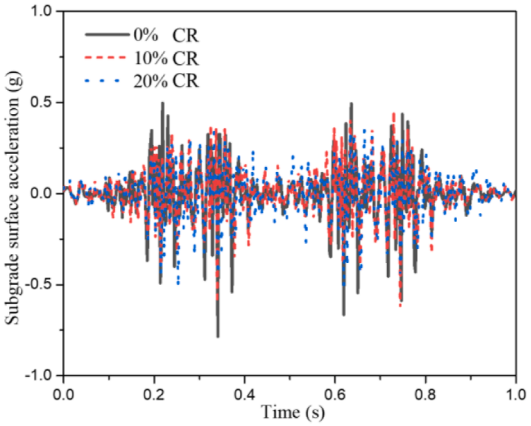

a. Subgrade surface acceleration at track position x = 0 m

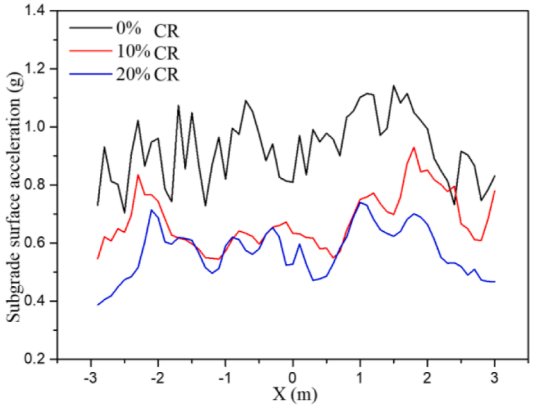

b. Subgrade surface acceleration amplitude at different track positions, CR size 8.0-22.4 mm

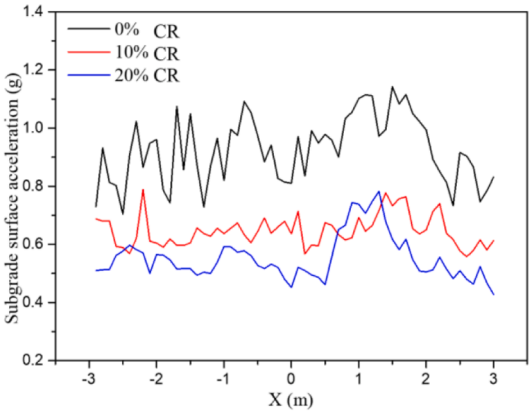

b. Subgrade surface acceleration amplitude at different track positions, CR size 9.5-63.0 mm

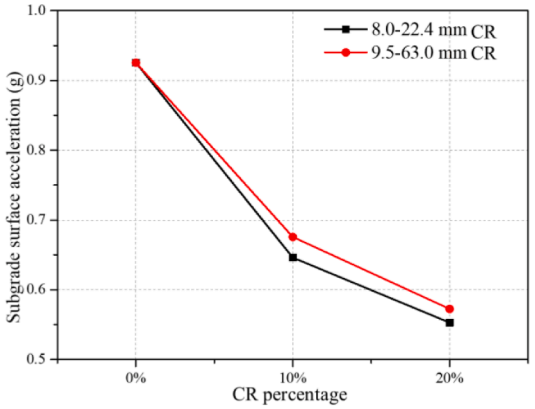

d. Average of subgrade surface acceleration amplitude of different CR percentages

Fig. 16. Subgrade surface acceleration under ballasted track with CR.

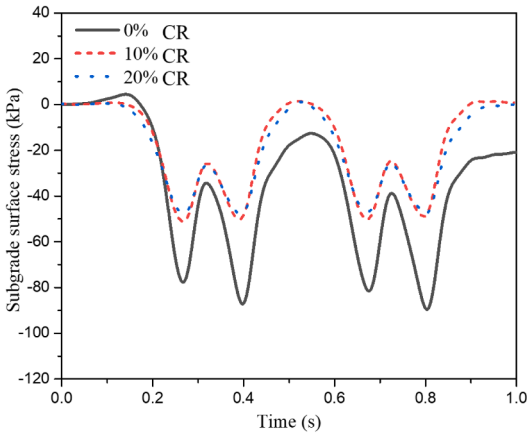

a. Subgrade surface stress at track position x = 0 m

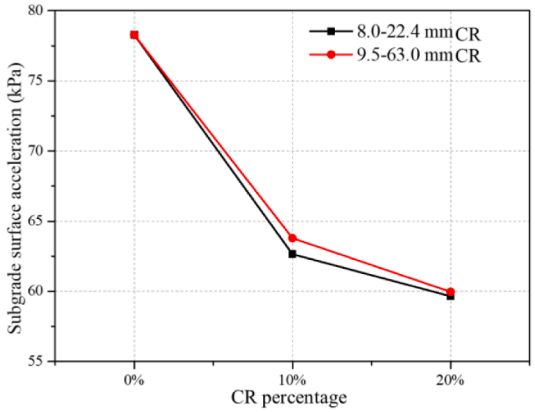

b. Average of subgrade surface stress of different CR percentages

Fig. 17. Subgrade surface stress under ballasted track with CR.

m) of different CR percentage are almost the same. Fig. 10b/c present the maximum rail dynamical bending moments when the vehicle was operating on different track positions. From the Fig. 10b/c, it can be seen that the maximum dynamical bending moments have few changes when applying the CR. This can also be seen in Fig. 10d, which presents the average value of the maximum bending moments of different CR percentages. It shows that the 10% and 20% CR (8.0–22.4 mm) increase the maximum bending moments by 0.4% and 4% than without CR, respectively. For the CR size at 9.5–63.0 mm, the maximum bending moments increase 1.5% (10% CR) and 3% (20% CR) than 0% CR, respectively.

Fig. 10 can demonstrate that the rail dynamical bending moments have few changes with CR, which is less than 4%. This means the CR can rarely change the rail bearing condition.

3.2.2. *Sleeper displacement*

Fig. 11 summaries the sleeper displacements on the conditions of different CR percentage and size. The sleeper displacements (CR size:

8.0–22.4 mm) at × = 0 m is shown in Fig. 11a, and it demonstrates that during the vehicle passing the sleeper displacements of different CR percentage have similar curve shape but with different magnitudes. Specifically, the maximum sleeper displacement without CR is 0.82, while with 10% and 20% are 1.34 mm and 1.51 mm, respectively. This proves that the CR can reduce the ballast bed stiffness.

Fig. 11b/c show the maximum sleeper displacements of different track positions with different CR percentages and sizes. It can be seen that the maximum values are almost the same, and the maximum sleeper displacement increases as the CR percentage increases.

Fig. 11d calculates the average value of maximum sleeper displacements at different track positions. It shows that higher CR percentage leads to higher average displacement value, and small size CR influences more than large size. Specifically, 10% and 20% 8.0–22.4 mm CR increase the average value by 57% and 114%, respectively, while by 51% and 108% were increased by 10% and 20% 9.5–63.0 mm CR, respectively.

3.2.3. Sleeper acceleration

Fig. 12 summaries the sleeper accelerations on the conditions of different CR percentages and sizes. Specifically, the sleeper accelerations (CR size 8.0–22.4 mm) at the track position × = 0 mm is shown in Fig. 12a, which shows that the sleeper acceleration increases as the CR percentage increases. The acceleration amplitude is 2.53 g without CR, and it is increased to 2.68 g and 2.90 g with the 10% and 20% CR, respectively.

Fig. 12b/c show the sleeper acceleration amplitudes at different track positions. From the figures, it can be seen that both small size CR (8.0–22.4 mm) and large size CR (9.5–63.0 mm) can increase the acceleration amplitude. In addition, the CR percentage has slight influence on the sleeper acceleration amplitude.

Fig. 12d presents the average of sleeper acceleration amplitudes. For the CR of 8.0–22.4 mm, the sleeper average value increases by 7% with 10% CR, and after that the average value increment is not obvious, which is only at 1% (CR from 10% to 20%). For the CR of 9.5–63.0 mm, 10% and 20% CR increase the average value by 6% and 9% than without CR, respectively.

From Fig. 12, it can be summarised that the CR can increase sleeper acceleration, and the increment is related to the CR percentage but little related to the CR size. Most importantly, the acceleration amplitude increment is within 10%, which is acceptable for considerations of ride safety and comfort.

3.2.4. Ballast acceleration

Fig. 13 summaries the ballast accelerations at x = 0 m, 150 mm below sleeper on the conditions of different CR percentages and sizes. Because in 2D DEM ballast layer model it is easy to find the particles at the same depth below the sleeper. The particles at almost the same positions were selected, because the accelerations of ballast particles at the similar positions can be similar. Because different ballast acceleration is caused by the ballast layer compaction difference and the coordination number difference (coordination number can be found in [48]). In addition, the ballast layer was compacted before applying the cyclic loadings, and we controlled the porosity of the ballast layer. We selected ballast particles with the very similar coordination numbers.

In that case, the only difference would be if the rubber is involved. Because the rubber can differ the ballast acceleration a lot, by as a buffer or affect ballast-ballast interaction. This means the ballast can have either more damping or less damping, which depends on the TDA size and percentage.

To be more specific, for Fig. 13a, ballast acceleration trends of different CR percentages (peak and valley points) are almost the same but with different magnitudes. In other words, 10% and 20% CR make the ballast accelerations at 2.31 g and 3.67 g, respectively, which are higher than ballast acceleration without CR, 2.01 g. It shows the 20% CR increases ballast acceleration much more than 10%.

Fig. 13b/c present the ballast acceleration amplitude at different track positions with different CR sizes and percentages. From the figure, it can be seen that using CR makes the ballast acceleration amplitudes have a wider range than without CR. However, it has slight influences on the ballast-CR track performance, due to the ballast acceleration (or energy) dissipated very fast (explained in 3.2.6).

Fig. 13d summaries the average value of ballast acceleration amplitude at different track positions with different CR sizes and percentages. The figure shows that the average values increase as the CR percentage. For the small size CR (8.0–22.4 mm), the average values were increased by 24% (10% CR) and 44% (20% CR), respectively. For the big size CR (9.5–63.0 mm), the average values were increased by 3% (10% CR) and 26% (20% CR), respectively. Fig. 13 demonstrates that 10% CR with size at 9.5–63.0 mm has the least acceleration change. This is possibly due to the big size CRs have the least chances to change the interactions between ballast particles, because 9.5–63.0 mm CR has large size, and with the same mass this makes the CR number fewer. Note that the CR percentage decides the ballast layer acceleration, which is closely related to the ballast layer destabilization. In addition, increasing ballast layer acceleration may accelerate ballast degradation. This is a disadvantage when using the CR at an inappropriate mass percentage.

3.2.5. Ballast bed stress

The ballast bed stress is obtained by setting a measuring circle (radius: 0.1 m) below the rail sleeper at a distance of 0.1 m from the top of the subgrade layer. The resultant force in the measuring circle and the circle area are used to calculate for the ballast bed stress. The function of the measuring circle has coordination number, stress, force and so on, which can be found more explanations in [59].

As shown in Fig. 14, the ballast bed stress of track with different size and percentage CR is summarised. The ballast bed stress can show the support condition of ballast bed under dynamic situations. It is calculated through the sleeper support forces and sleeper bottom area.

Fig. 14a shows ballast bed stress at track position x = 0 m with different percentages of CR. The figure shows that the stress curve shapes are similar but with different magnitudes. Specifically, the stress was reduced from 119 kPa (without CR) to 80 kPa (10% CR) and 74 kPa (20% CR), respectively.

Fig. 14b/c summary the maximum ballast bed stress at different track positions with different CR sizes and percentages. The figures present that the maximum ballast bed stress reduces when applying the CR, and small size CR (8.0–22.4 mm) has uniform ballast bed stress from 70 to 100 kPa. While big size CR (9.5–63.0 mm) has wider range at 50–130 kPa. This is due to small size CR can make homogeneous mixing of ballast and CR. This trend seems to be majorly attributed to the further accommodation facilitation of smaller-sized CR among coarse-sized ballast particles, which could lead to the further stress improvement of mixture.

Fig. 14d presents the average value of ballast bed stress at different track positions. The figure shows that for small size CR (10%), the average value reduces by 37% than without CR, while CR percentage increases from 10% to 20%, the average value only reduces by 1%. The average value reduction for big size CR (9.5–63.0 mm) is also the same trend, specifically, 29% (CR from 0% to 10%) and 8% (CR from 10% to 20%). From this, it can be seen that 10% CR is already enough to reduce ballast bed stress, after over 10% increasing the percentage has not obvious effects.

3.2.6. Ballast friction energy dissipation

The ballast friction energy dissipation is calculated by Eq. (3). In the equation, E_μ is the ballast friction energy dissipation; $(F_s^l)_0$ is the initial shear force at the contact; F_s^l is the shear force after one time step; $\Delta\delta_s^\mu$ is the slide displacement at the contact in one time step. The total E_μ at all ballast-ballast contacts are the friction energy dissipation. More

explanations about the friction energy dissipation can be found in [59].

$$E_u = \frac{1}{2}\left(\left(F_s^l\right)_0 + F_s^l\right)\cdot\Delta\delta_s^u \quad (3)$$

Fig. 15 summaries ballast friction energy dissipation of ballasted track with different CR sizes and percentages. The ballast friction energy dissipation presents the energy amounts that are dissipated by the friction between ballast particles. Fig. 15a shows the ballast friction energy dissipation of small size CR (8.0–22.4 mm), and the detailed numbers are 613 J (0% CR), 94 J (10% CR) and 100 J (20% CR). It means using CR can reduce ballast relative abrasion and then reducing degradation. We compared the energy dissipation by CR with the results in [28]. The dissipated energy by 10% CR is 613–94 = 519 J, and the track length is 8.4*2.6*0.35 m^3 with 13 sleepers, which makes the final result 35 J/m^3. The result is comparable to the result in [28], around 40 J.

Fig. 15b shows the ballast friction energy dissipation of ballasted track with different sizes and percentages. Specifically, as the 8.0–22.4 mm CR percentage increases from 0 to 10%, the energy dissipation reduces 85%, and for the 9.5–63.0 mm the number is 80%. However, as the CR percentage increase from 10% to 20%, the energy dissipation reduction is not obvious. In addition, the CR size has few influences on the energy dissipation.

Particularly, the breakage of ballast particles was also considered in these simulations. It was found that when using the CR, no ballast breakage was found. But without CR the ballast breakage was clear shown. Each ballast particle in our DEM model was made by bonding several discs together through parallel bonds. The ballast breakage was presented by the parallel bond breakage. After the simulation process, we checked the breakage number of the parallel bonds, which is the reflection of ballast breakage. From the breakage number comparison, it shows using CR can significantly reduce ballast breakage, which is also proved by the study in [29].

3.3. Subgrade dynamic performance

3.3.1. Subgrade surface acceleration

Fig. 16 shows subgrade surface acceleration of ballasted track with different CR sizes and percentages. The acceleration is measured at below each sleeper at the subgrade surface. Specifically, as shown in Fig. 16a, at the position x = 0 m, the surface acceleration without CR is 0.81 g, which is reduced to 0.63 g (10% CR) and 0.52 g (20% CR), respectively. This means using CR improves the dynamic performance of subgrade. This is also demonstrated by Fig. 16 b/c, which present the subgrade surface acceleration amplitudes at different track positions with different CR sizes and percentages. From Fig. 16d, it can be seen increasing from 0% to 10% percentage CR reduces the acceleration much more significantly than from 10% to 20%, which means 10% percentage CR is sufficient to provide good dynamic performance of subgrade.

3.3.2. Subgrade surface stress

Fig. 17 summaries the subgrade surface stress of ballasted track with different CR sizes and percentages. Fig. 17a shows the subgrade surface stress at the track position x = 0 m with 8.0–22.4 mm CR. From the figure, it demonstrates that using CR can reduce the subgrade surface stress (peak value) from 92 kPa to 52 kPa and 49 kPa (10% or 20% CR), respectively. This can also be observed in Fig. 17b, which also shows that increasing CR percentage from 10% to 20% has much less significant reduction than from 0% to 10%. This means 10% CR is sufficient for subgrade surface stress reduction, and CR size has little influence on the reduction.

4. Conclusions and perspectives

4.1. Conclusions

This paper aimed at studying dynamic performance of ballasted track with crumb rubber (CR). In this regard, a coupled model that includes multibody dynamics part, discrete element method part and finite difference method part was built, and some important dynamic performance of the whole system (vehicle-track-subgrade) was obtained and analysed, including the vehicle body acceleration, wheel-rail force, rail dynamical bending moment, sleeper acceleration, sleeper displacement and ballast acceleration. Two factors, the CR size and percentage, were considered. Through the dynamic performance analysis, the conclusions were draw as follows.

1. Using CR has little influence on the car body acceleration, wheel-rail contact and rail dynamical bending moment, which means it does not affect ride comfort and safety.
2. Using CR influences dynamic performance of ballasted track very much, including sleeper acceleration increase, ballast acceleration amplitude increase and ballast bed stress reduction. However, ballast degradation (abrasion and breakage) is considerably reduced.
3. Using CR significantly reduces subgrade surface vibration and stress, which is helpful for reducing long-term plastic deformation.
4. 10% percentage of CR-ballast mixture is recommended, and for CR size it is difficult to give a recommendation. Because small size CR increase ballast acceleration more than big size CR, but small size CR are better at other aspects, including sleeper displacement, subgrade stress and ballast bed stress.

4.2. Perspectives

The applied coupled models are in two-dimensional, because the computational costs are too expensive. For example, current model takes around one week to calculate one train passing (1.2 s) with the computer of 20 parallel threads. 3D coupled models will be considered in the future for more accurate analysis using the high-performance computer.

CRediT authorship contribution statement

Yunlong Guo: Writing – original draft, Writing – review & editing. **Can Shi:** Formal analysis, Investigation, Software, Visualization, Data curation. **Chunfa Zhao:** Supervision, Funding acquisition, Resources. **Valeri Markine:** Supervision. **Guoqing Jing:** Supervision, Resources.

Declaration of Competing Interest

The authors declare that they have no known competing financial interests or personal relationships that could have appeared to influence the work reported in this paper.

Acknowledgement

This is from work undertaken as part of the IN2ZONE project, which has received funding from the Shift2Rail Joint Undertaking (JU) under grant agreement 101014571 – IP/ITD/CCA – IP3. We also would like to acknowledge the support of the Chinese Program of Introducing Talents of Discipline to Universities (111 Project, Grant No. B16041) and the National Natural Science Foundation of China (Grant No. 51578469). The support from China Railway Construction Corporation (science and technology planning project, grant No. crcce-tec-2019-0052) is also acknowledged.

References

[1] B. Indraratna, W. Salim, C. Rujikiatkamjorn, Advanced Rail Geotechnology: Ballasted Track, CRC Press London, 2011.

[4] M. Przybyłowicz, M. Sysyn, U. Gerber, V. Kovalchuk, S. Fischer, Comparison of the effects and efficiency of vertical and side tamping methods for ballasted railway tracks, Constr. Build. Mater. 314 (2022).
[5] Y. Guo, V. Markine, X. Zhang, W. Qiang, G. Jing, Image analysis for morphology, rheology and degradation study of railway ballast: A review, Transp. Geotech. 18 (2019) 173–211.
[6] B. Standard, BS EN 13450 (2002), Aggregates for railway ballast.
[9] T.P.M.o. Railways, Railway Ballast, TB/T2140-2008, China Railway Publishing House, Beijing, 2008.
[10] A.R.E. Association, Manual for Railway Engineering 1995, American Railway Engineering Association, 1995.
[11] J. Qian, J. Gu, X. Gu, M. Huang, L. Mu, DEM analysis of railtrack ballast degradation under monotonic and cyclic loading, Procedia Eng. 143 (2016) 1285–1292.
[12] N.T. Ngo, B. Indraratna, C. Rujikiatkamjorn, M. Mahdi Biabani, Experimental and discrete element modeling of geocell-stabilized subballast subjected to cyclic loading, J. Geotech. Geoenviron. Eng. 142 (4) (2016) 04015100.
[13] M. Koohmishi, A. Azarhoosh, Hydraulic conductivity of fresh railway ballast mixed with crumb rubber considering size and percentage of crumb rubber as well as aggregate gradation, Constr. Build. Mater. 241 (2020), 118133.
[14] C. Ngamkhanong, B. Feng, E. Tutumluer, Y.M.A. Hashash, S. Kaewunruen, Evaluation of lateral stability of railway tracks due to ballast degradation, Constr. Build. Mater. 278 (2021).
[15] Q. Sun, B. Indraratna, S. Nimbalkar, An elasto-plastic method for analysing the deformation of the railway ballast, Procedia Eng. 143 (2016) 954–960.
[16] B. Indraratna, Y. Sun, S. Nimbalkar, Laboratory assessment of the role of particle size distribution on the deformation and degradation of ballast under cyclic loading, J. Geotech. Geoenviron. Eng. 142 (7) (2016) 04016016.
[17] R. Müller, Under Ballast Mats (UBM) Insertion Loss, UIC-Report, Version 3, 2008, p. 04.
[18] C. Chen, G.R. McDowell, N.H. Thom, Discrete element modelling of cyclic loads of geogrid-reinforced ballast under confined and unconfined conditions, Geotext. Geomembr. 35 (2012) 76–86.
[19] G.Q. Jing, L.C. Qie, V. Markine, W.L. Jia, Polyurethane reinforced ballasted track: Review, innovation and challenge, Constr. Build. Mater. 208 (2019) 734–748.
[20] C. Ngamkhanong, S. Kaewunruen, Effects of under sleeper pads on dynamic responses of railway prestressed concrete sleepers subjected to high intensity impact loads, Eng. Struct. 214 (2020).
[21] M. Sol-Sánchez, F. Moreno-Navarro, M.C. Rubio-Gámez, Viability of using end-of-life tire pads as under sleeper pads in railway, Constr. Build. Mater. 64 (2014) 150–156.
[22] M. Fathali, F.M. Nejad, M. Esmaeili, Influence of tire-derived aggregates on the properties of railway ballast material, J. Mater. Civ. Eng. 29 (1) (2017) 04016177.
[23] S. Wolfe, D. Humphrey, Vibration attenuation of tire shreds. Rail Transit Conference, 2000, 2000.
[24] C. Hidalgo Signes, P. Martínez Fernández, E. Medel Perallón, R. Insa Franco, Characterisation of an unbound granular mixture with waste tyre rubber for subballast layers, Mater. Struct. 48 (12) (2014) 3847–3861.
[25] C. Hidalgo Signes, P. Martínez Fernández, E. Medel Perallón, R. Insa Franco, Analysis of the vibration alleviation of a new railway sub-ballast layer with waste tyre rubber, Mater. Struct. 50 (2) (2016).
[26] P. Martínez Fernández, C. Hidalgo Signes, I. Villalba Sanchís, D. Pérez Mira, R. Insa Franco, Real scale evaluation of vibration mitigation of sub-ballast layers with added tyre-derived aggregate, Constr. Build. Mater. 169 (2018) 335–346.
[27] Y. Qi, B. Indraratna, A. Heitor, J.S. Vinod, Effect of rubber crumbs on the cyclic behavior of steel furnace slag and coal wash mixtures, J. Geotech. Geoenviron. Eng. 144 (2) (2018).
[28] M. Sol-Sánchez, N.H. Thom, F. Moreno-Navarro, M.C. Rubio-Gámez, G.D. Airey, A study into the use of crumb rubber in railway ballast, Constr. Build. Mater. 75 (2015) 19–24.
[29] H. Gong, W. Song, B. Huang, X. Shu, B. Han, H. Wu, J. Zou, Direct shear properties of railway ballast mixed with tire derived aggregates: Experimental and numerical investigations, Constr. Build. Mater. 200 (2019) 465–473.
[30] M. Fathali, M. Esmaeili, F. Moghadas Nejad, Influence of tire-derived aggregates mixed with ballast on ground-borne vibrations, Journal of Modern, Transportation (2019).
[31] M. Esmaeili, M. Siahkouhi, Tire-derived aggregate layer performance in railway bridges as a novel impact absorber: Numerical and field study, Struct. Control Health Monit. (2019).
[32] M. Esmaeili, H. Ebrahimi, M.K. Sameni, Experimental and numerical investigation of the dynamic behavior of ballasted track containing ballast mixed with TDA, Proc. Inst. Mech. Eng., Part F: J. Rail Rapid Transit 232 (1) (2016) 297–314.
[33] W. Zhai, Vehicle–Track Coupled Dynamics Theory and Applications, Springer, Singapore, 2020.
[34] W. Zhai, K. Wang, C. Cai, Fundamentals of vehicle–track coupled dynamics, Veh. Syst. Dyn. 47 (11) (2009) 1349–1376.
[35] W. Zhai, K. Wang, J. Lin, Modelling and experiment of railway ballast vibrations, J. Sound Vib. 270 (4) (2004) 673–683.
[36] W. Zhai, X.J.v.s.d. Sun, A detailed model for investigating vertical interaction between railway vehicle and track, 23(sup1) (1994) 603-615.
[37] W.M. Zhai, Two simple fast integration methods for large-scale dynamic problems in engineering, Int. J. Numer. Meth. Eng. 39 (24) (1996) 4199–4214.
[38] C. Shi, Study on Macro-Meso Dynamic Mechanical Behaviour of Railway Ballasted Track and Infrastructures, Southwest Jiaotong University, Chengdu, 2020.
[39] C. Shi, C. Zhao, X. Zhang, Y. Guo, Coupled discrete-continuum approach for railway ballast track and subgrade macro-meso analysis, Int. J. Pavement Eng. (2020) 1–16.
[40] P.A. Cundall, O.D. Strack, A discrete numerical model for granular assemblies, Geotechnique 29 (1) (1979) 47–65.
[41] G.R. McDowell, W.L. Lim, A.C. Collop, R. Armitage, N.H. Thom, Laboratory simulation of train loading and tamping on ballast, in: Proceedings of the Institution of Civil Engineers-Transport, Thomas Telford Ltd, 2005, pp. 89-95.
[42] E. Tutumluer, Y. Qian, Y.M.A. Hashash, J. Ghaboussi, D.D. Davis, Discrete element modelling of ballasted track deformation behaviour, Int. J. Rail Transp. 1 (1–2) (2013) 57–73.
[43] B. Indraratna, S.S. Nimbalkar, N.T. Ngo, T. Neville, Performance improvement of rail track substructure using artificial inclusions – Experimental and numerical studies, Transp. Geotech. 8 (2016) 69–85.
[44] J.-L. Xiao, G.-Z. Liu, J.-X. Liu, J.-C. Dai, H. Liu, P. Wang, Parameters of a discrete element ballasted bed model based on a response surface method, J. Zhejiang Univ.-SCIENCE A 20 (9) (2019) 685–700.
[45] J. Harkness, A. Zervos, L. Le Pen, S. Aingaran, W. Powrie, Discrete element simulation of railway ballast: modelling cell pressure effects in triaxial tests, Granular Matter 18 (3) (2016) 1–13.
[46] Y. Guo, C. Zhao, V. Markine, G. Jing, W. Zhai, Calibration for discrete element modelling of railway ballast: A review, Transp. Geotech. 23 (2020), 100341.
[47] O. Harireche, G.R. McDowell, Discrete element modelling of cyclic loading of crushable aggreates, Granular Matter 5 (3) (2003) 147–151.
[48] S. Lobo-Guerrero, L.E. Vallejo, Discrete element method analysis of railtrack ballast degradation during cyclic loading, Granular Matter 8 (3–4) (2006) 195–204.
[50] Z. Hossain, B. Indraratna, F. Darve, P. Thakur, DEM analysis of angular ballast breakage under cyclic loading, Geomech. Geoeng. 2 (3) (2007) 175–181.
[51] G. Saussine, C. Cholet, P.E. Gautier, F. Dubois, C. Bohatier, J.J. Moreau, Modelling ballast behaviour under dynamic loading. Part 1: A 2D polygonal discrete element method approach, Comput. Methods Appl. Mech. Eng. 195 (19–22) (2006) 2841–2859.
[52] G.R. McDowell, H. Li, Discrete element modelling of scaled railway ballast under triaxial conditions, Granular Matter 18 (3) (2016).
[53] B.s.p.B.E British Standards Institution, Aggregates for railway ballast, British Standards Institution, London, 2013.
[54] N.T. Ngo, B. Indraratna, C. Rujikiatkamjorn, Simulation ballasted track behavior: numerical treatment and field application, Int. J. Geomech. 17 (6) (2016) 04016130.
[55] M. Cai, P. Kaiser, H. Morioka, M. Minami, T. Maejima, Y. Tasaka, H. Kurose, FLAC/PFC coupled numerical simulation of AE in large-scale underground excavations, Int. J. Rock Mech. Min. Sci. 44 (4) (2007) 550–564.
[56] L. Li, W. Liu, M. Ma, G. Jing, W. Liu, Research on the dynamic behaviour of the railway ballast assembly subject to the low loading condition based on a tridimensional DEM-FDM coupled approach, Constr. Build. Mater. 218 (2019) 135–149.
[57] Y. Guo, Application of new materials and elements to railway ballasted track for performance improvement, (2021).
[58] X. Zhang, C. Zhao, W. Zhai, Dynamic behavior analysis of high-speed railway ballast under moving vehicle loads using discrete element method, Int. J. Geomech. 17 (7) (2016) 04016157.
[59] C. Itasca, PFC (particle flow code in 2 and 3 dimensions), version 5.0 [User's manual], Minneapolis, 2014.